RSC Advances

PAPER

View Article Online
View Journal | View Issue

Cite this: *RSC Adv.*, 2020, **10**, 41264

Synthesis and electronic properties of pyridine end-capped cyclopentadithiophene-vinylene oligomers†

Fernando G. Guijarro, ‡[a] Samara Medina Rivero, ‡[b] Suman Gunasekaran,[c] Iratxe Arretxea,[b] Rocío Ponce Ortiz,[b] Rubén Caballero,[a] Pilar de la Cruz,[a] Fernando Langa, *[a] Latha Venkataraman *[cd] and Juan Casado *[b]

A series of four oligomers of cyclopentadithiophene-vinylenes end capped with pyridine groups was prepared and their optical and electronic properties studied. Treatment with trifluoroacetic acid (TFA) leads to the bisprotonation of the nitrogens of the pyridine, which has an important impact on the optical properties. Excess treatment with TFA provokes the oxidation of the conjugated core, generating radical cations and dications. The ease of the TFA treatment in solution was extended to protonation in the solid-state where further characterization of the neutral and TFA-treated samples was carried out in electrically active substrates in organic field-effect transistors. Finally, the new molecules were found to be excellent conductors in single-molecule junctions thanks to strong electron delocalization and resonance orbital mediated transport. These studies show the opening of a spectrum of possibilities by suitable terminal substitution of π-cores.

Received 25th September 2020
Accepted 1st November 2020

DOI: 10.1039/d0ra08220a

rsc.li/rsc-advances

Introduction

Oligomers of cyclopentadithiophene-vinylenes (***n*CPDTVs**) possess a longer mean conjugation length than their closely related oligothiophene-vinylenes (***n*TVs**),[1] and much longer than the chemically uniform oligothiophenes (***n*Ts**). This is a positive starting point for the design of new functionalized ***n*CPDTVs** with an eye towards improved and diversified electronic applications. However, surprisingly, the variety of synthetic designs and structures based on ***n*CPDTVs** is significantly smaller than for ***n*TV**[2] or ***n*Ts**.[3] For instance, typical ***n*TV**/***n*T** have been extended with *ad-hoc* terminal functionalization in many different oligomeric families;[3] however, these variants of ***n*CPDTVs** have been scarcely taken into account. Conversely to the case of the oligomers, the **CPDTV** unit monomer has been intensively used in co-polymer designs providing excellent solid-state field effect transistor (FET) mobilities[4–7] and high performance in polymer-based organic solar cells.[8–11] Notable compounds in the family of π-conjugated oligomers based on ***n*CPDTVs** include the trimeric cyclic **CPDTV**[12,13] and the quinoidal tetracyano **CPDTV** compound.[1] We have also reported the unsubstituted series of ***n*CPDTVs**.[1] The chemical structures of these **CPDTV** based oligomers are represented in Scheme 1.

Terminal encapsulation of the π-electronic structure of the wire oligomers has been often considered in order to preserve the central π-conjugated unit from terminal ring reactivity; however, it can be also exploited to impart new and diversified electronic functionalities, for instance: (i) terminal disubstitution of π-conjugated oligomers with thioalkyl groups provides the molecules with the ability to bind gold for single molecular conductance measurements;[14,15] or (ii) disubstitution

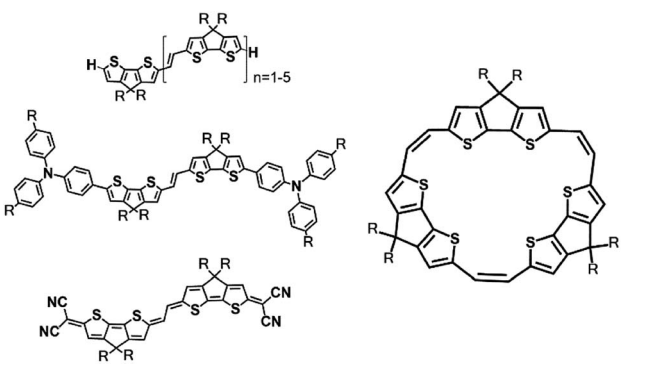

Scheme 1 Chemical structures of the most distinctive **CPDTV** based oligomers (R = hexyls) studied.

[a]*Instituto de Nanociencia, Nanotecnología y Materiales Moleculares (INAMOL), Universidad de Castilla-La Mancha, Toledo, Spain*

[b]*Department of Physical Chemistry, University of Malaga, Campus de Teatinos s/n, 229071 Malaga, Spain. E-mail: casado@uma.es*

[c]*Department of Chemistry, Columbia University, New York 10027, USA*

[d]*Department of Applied Physics and Applied Mathematics, Columbia University, New York 10027, USA*

† Electronic supplementary information (ESI) available. See DOI: 10.1039/d0ra08220a

‡ These authors contributed equally to this work.

with electro-active groups could supply additional/enhanced photophysical and chemical properties, *etc.*[2,3]

It has been over 30 years since the first utilization of π-conjugated oligomers in electronic applications.[16] Since then, a lot of different applications have been developed, such as organic field effect transistors (OFET),[17] organic light emitting diodes,[18] organic photovoltaics,[19] sensors,[20] *etc.* These applications are based on the modulation of the electronic band gap by the number of repeating units in the π-conjugated backbone and the straightforward influence in the energy of the HOMO and LUMO molecular orbitals, which determine to a large extent the semiconducting property, the color of emitted light, its efficiency, *etc.* These are all bulk applications of π-conjugated oligomers, but single molecule-based electronic devices have been also developed since the pioneering work by Tour *et al.*[15]

In this paper, we have developed a new series of ***n*CPDTV** oligomers with pyridine end-caps (*i.e.*, **Py*n*CPDTV** in Scheme 2). This seemingly simple chemical design provides a wide array of different properties. In particular, the lone electron pair of the nitrogen provides a new venue of chemical and electronic diversity and tunability. For instance, we show that these lone pairs can be protonated in an acid–base reaction. Furthermore, proton exchange is compatible with the typical redox properties of conjugated oligomers consisting in the addition/extraction of π-electrons and this is carried out by the same agent which opens the possibility of dual doping of the semiconducting substrates. We report the construction of OFET devices, exploiting the synergy between the proton activity and redox. In addition, given the ability of the pyridine nitrogens to bind to gold, we have carried out single-molecule conductance measurements.

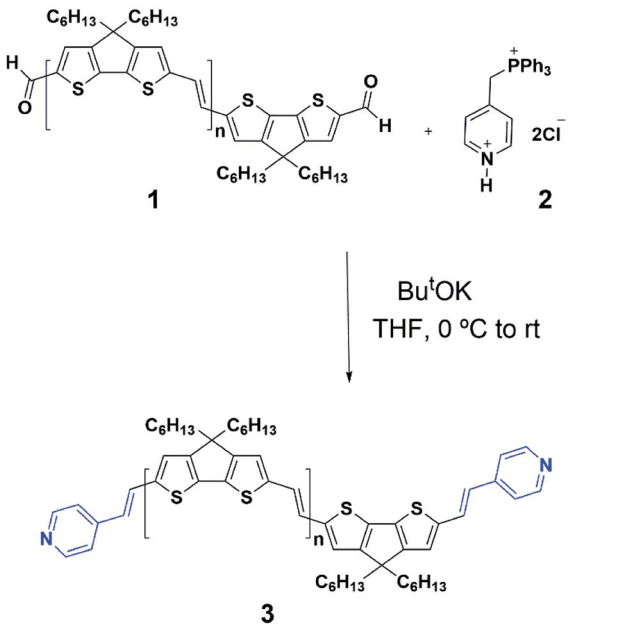

Scheme 2 Synthesis of the **Py*n*CPDTV** oligomers, with n = 0 (**Py1CPDTV**), with $n = 1$ (**Py2CPDTV**), with $n = 2$ (**Py3CPDTV**) and with $n = 3$ (**Py4CPDTV**).

Synthesis and experimental details

Synthesis

Scheme 2 summarizes the general synthesis of the four compounds.

Py*n*CPDTV by Wittig reaction between bisaldehydes **1a–d**[1] and the ylides generated from 4-((triphenylphosphonio)methyl) pyridin-1-ium dichloride **2**[21] and $Bu^tO^-K^+$; after purification by column chromatography followed by GPC, **Py*n*CPDTV** (**3a–d**) were obtained in 64–81% yield (see ESI file, Scheme S1,† for details). The chemical structures of all new compounds were verified by ^{1}H NMR, ^{13}C NMR, FT-IR and MALDI-TOF MS (for Experimental details and spectra see the ESI, Fig. S1–S27†). Purity was checked by HPLC (see the ESI, Fig. S7, S14, S21 and S28†). Compounds **Py*n*CPDTV** displayed simple, well-resolved ^{1}H NMR spectra in agreement with their structures. The presence of the pyridine moieties is evidenced by two duplets at around 7.3 ppm and 9.5 ppm.

Spectroscopic details

Absorption spectra were recorded with a Cary 5000 spectrophotometer from Varian operating in a maximal 175–3300 nm range. The 1064 nm FT-Raman spectra were obtained with a FT-Raman accessory kit (FRA/106-S) of a Bruker Equinox 55 FT-IR interferometer. A continuous-wave Nd-YAG laser working at 1064 nm was employed for excitation. A germanium detector operating at liquid nitrogen temperature was used. Raman scattering radiation was collected in a back-scattering configuration with a standard spectral resolution of 4 cm^{-1}. 1000–3000 scans were averaged for each spectrum.

Electrochemical and spectroelectrochemical details

Electrochemical experiments were conducted in *o*-DCB/acetonitrile (4 : 1) at room temperature by using 0.1 M tetrabutyl ammonium perchlorate, Bu_4NClO_4, as the supporting electrolyte. A glassy carbon was used as the working electrode and a Pt wire as the auxiliary electrode against a pseudo-reference electrode of Ag/0.01 M $AgNO_3$. All redox potentials provided are referred to the Fc/Fc^+ pair. Oxidized species were generated in CH_2Cl_2 solutions by progressive addition of $FeCl_3$ and/or trifluoroacetic acid, TFA.

Theoretical calculations

Quantum-chemical calculations were done in the framework of the density functional theory as implemented in the Gaussian'16 package.[22] Simulations were performed in the gas-phase. The B3LYP exchange-correlational functional[23] and the 6-31G** basis set[24] were used in all calculations.

Transistor fabrication and characterization

Field-effect transistors were fabricated by deposition from drop-coating or spin coating methods from tetrahydrofuran solutions over previously OTS treated SiO_2 surfaces and the films were annealed at 80 °C. The as-deposited compounds were exposed to the TFA vapors from a solution of TFA. On these films (both pristine and TFA doped), the OFET measurements

were conducted. Prior to deposition, the wafers were cleaned by rinsing twice with EtOH followed by a 10 min plasma cleaning in a Harrick PDC-32G Plasma Cleaner/Sterilizer. Then, a self-assembled monolayer (SAM) of either hexamethyldisilazane (HMDS) or octadecyltrichlorosilane (OTS) was deposited in order to reduce charge trapping and thus enhance device characteristics. Treatment with octadecyltrichlorosilane was performed by immersing the silicon wafers in a 3.0 mM humidity-exposed OTS-hexane solution for 1 hour, as previously described.[25] After OTS deposition, the substrates were sonicated with hexane, acetone and ethanol for 10 min each, and finally dried with a nitrogen stream. After semiconductor deposition, the solution-processed films were annealed under vacuum at 80 °C for 60 min. The fabrication of the devices was completed by gold electron vapor deposition using shadow masks with different channel lengths and channel widths. Devices were characterized under ambient conditions in an EB-4 Everbeing probe station with a 4200-SCS/C Keithley semiconductor characterization system.

Single-molecule conductance measurements

Single-molecule conductance measurements of **Py*n*CPDTV** were performed using the scanning tunneling microscope break junction technique (STM-BJ)[26] as described previously.[27] In this technique, a gold tip is placed in proximity to a gold substrate in a solution of the analyte. Measurements herein were performed in 0.1 mM solutions in 1-bromonaphthalene. For each measurement, the gold tip is pressed into the substrate until a conductance of 5 G_0 is reached ($G_0 = 2e^2/h$). The tip is then retracted, allowing a small, atomically-defined gap to form between the tip and substrate. A single **Py*n*CPDTV** molecule, by means of the pyridine end-caps, can bridge this gap and form a single-molecule junction. The conductance (current/voltage) is recorded during the retraction, and a single-molecule junction manifests itself as a plateau-like feature below 1 G_0 in the conductance *versus* displacement trace. Several thousand conductance traces are recorded and plotted in logarithmically-binned one-dimensional (1D) conductance histograms (100 bins/decade) as well as two-dimensional (2D) histograms of conductance *versus* displacement.

Results

Electrochemical and optical properties and electronic structure

Electrochemical properties. Electrochemical studies, using cyclic voltammetry (CV) and Osteryoung square-wave voltammetry (OSWV), were performed to gain insight into the redox behavior of **Py*n*CPDTV** (Tables 1, S1 and Fig. S29–S36†). In the cathodic region, the first reduction potential is observed at around −2.10 V in all oligomers and is attributed to the reversible reduction mainly controlled by both endcap pyridine moieties. In the anodic side, the first oxidation potential decreases from +0.80 V (**Py1CPDTV**) to −0.08 V (**Py4CPDTV**) as the length of the oligomer increases indicating the progressive destabilization of the HOMO orbitals from which the electrons are extracted.

These electrochemical data are in agreement with theoretical data from calculations in Fig. 1. Pyridine substitution on **2CPDTV → Py2CPDTV** stabilizes the LUMO orbital in line with the appearance of reduction in the pyridyl series. Furthermore, there is a small modulation of the LUMO energy in the **Py*n*CPDTV** series which agrees with the small changes in the reduction potential values. Finally, the HOMO orbital energies (Fig. S37†) are largely affected by the chain extension which explains the larger variation of the oxidation potentials in the series (Table S1†).

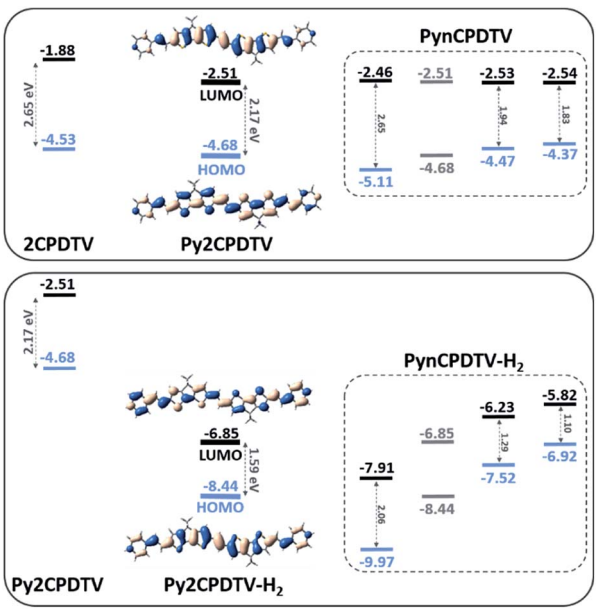

Fig. 1 (Top) DFT/B3LYP/6-31G** energies and topologies of the HOMO and LUMO orbitals of the compounds under study as neutrals (including the uncapped 2CPDTV). (Bottom) Upon bisprotonation.

Table 1 Optical data and redox potentials measured by OSWV (*versus* Fc/Fc^+)

	λ_{abs}[a] (nm)	log ε	λ_{abs}[a,b] (nm)	E_{ox}[1c] (V)	E_{red}[1c] (V)	E_{HOMO}[d] (eV)	E_{LUMO}[e] (eV)
Py1CPDTV	450	4.46	584	0.80	−2.13	−5.90	−2.97
Py2CPDTV	528	4.89	643	0.17	−2.12	−5.27	−2.98
Py3CPDTV	564	5.02	595	−0.01	−2.14	−5.11	−2.96
Py4CPDTV	584	5.16	644	−0.08	−2.12	−5.18	−2.98

[a] 10^{-6} M in dichloromethane. [b] **Py*n*CPDTV**–H_2. [c] 10^{-3} M in *o*-DCB–acetonitrile (4 : 1) *versus* Fc/Fc^+ glassy carbon, Pt counter electrode, 20 °C, 0.1 M Bu_4NClO_4, scan rate = 100 mV s^{-1}. [d] Estimated from $E_{HOMO} = -5.1 - E_{ox}^1$. [e] Estimated from $E_{LUMO} = -5.1 - E_{red}^1$. The E_{red} and E_{ox} were expressed *vs.* Fc/Fc^+ used as external reference.

Optical properties in solution: protonation. Fig. 2 shows the electronic absorption spectra of the three compounds in neutral state as well as upon protonation with trifluoroacetic acid (TFA) and Table 1 summarizes the main data. The lowest energy absorption bands of the electronic spectra of the four pristine compounds display a red-shift with increasing molecular size, as typically found in the unsubstituted **CPDTV**[1] parent oligomers. These absorptions can be mainly assigned to the mono-electronic transitions from the highest occupied molecular orbital to the lowest unoccupied molecular orbital (*i.e.*, HOMO-to-LUMO excitation). The narrowing of the HOMO–LUMO gap discussed previously in Fig. 1 explains the observed red-shift of the optical bands. The incorporation of terminal vinyl-pyridine groups (*i.e.*, regarding the central **CPDTV** core) produces a significant red-shift of the absorption bands which amount to +23 nm in the case of **Py4CPDTV** compared with the homologous compound with four **CPDTV** units,[1] **4CPDTV**.

Treatment of **Py1CPDTV** with TFA in solution in Fig. 2 leads to the sequential protonation of the nitrogens of the pyridines resulting in an electronic absorption spectrum of **Py1CPDTV** with a red-shifted band at 532 nm from 454 nm in the unprotonated species after first protonation, followed by a posterior shift to 584 nm due to the second protonation. These changes in the spectra upon acid reaction are consistent with the larger electron-accepting character of the pyridylium moieties imparting a CT character to the optical excitations originating the observed red-shifts. In the longer compounds, in TFA excess, protonation directly produces the doubly protonated species (*i.e.*, due to the minimization of the charge repulsion between the protonated nitrogens).

Optical properties in solution: oxidation. Treatment with TFA not only produces the protonation of the pyridyl nitrogens but, when added in excess, also gives rise to the appearance of new species with strong absorptions in the Vis-NIR spectral region (Fig. 2, S38 and Table S2†). To identify the origin of these species, we carried out chemical oxidation with $FeCl_3$ (also in Fig. 2) and found out that initial amount of $FeCl_3$ treatment produces exactly the same spectra as in the initial steps of the treatment with TFA (Fig. S39 and Table S3†). This can be understood by assuming that Fe(III) initially coordinates to the lone electron pair of the nitrogens giving rise to a spectrum similar to that upon protonation (*i.e.*, the differences due to the different Lewis acidity of the protons and of the Fe(III)). For instance, 643 nm for the main band of **Py2CPDTV** upon treatment with TFA acid and 675 nm for **Py2CPDTV** upon treatment (first process) with $FeCl_3$.

Further stepwise addition of $FeCl_3$ to the solution of the bi-coordinated **Py2CPDTV** produces the disappearance of the band at 675 nm and the growth of a strong band at 898 nm accompanied by a second absorption at 1470 nm, a two-bands pattern commonly found in the spectra of the radical cations of π-conjugated oligomers. This 898/1470 nm pattern obtained with $FeCl_3$ is very similar to that obtained upon addition of excess of TFA to bisprotonated **Py2CPDTV**, which equally consists on a two-bands pattern at 888/1260 nm. This comparison reveals the oxidant character of TFA which is able to additionally oxidize the π-electronic structure of the **Py2CPDTV** giving rise to the formation of the radical cationic forms. This is clearly seen also in the case of **Py3CPDTV** in which the bisprotonated sample upon further addition of TFA acid produces a new species with a two-bands spectral pattern at 1023 and 1784 nm which closely correlates with the bands at 1122 and 2076 nm in the TFA obtained radical cation of **Py4CPDTV**.

The oxidative reaction of TFA progresses beyond the first oxidized species and in **Py3CPDTV** a second species is obtained with two main bands at 1332 nm accompanied with another one at 846 nm (a similar spectrum is obtained by chemical oxidation of the radical cation with $FeCl_3$). The 1332 nm band perfectly correlates with the strong absorption feature at 1157 nm in the dication of the homologous compound without vinyl-pyridine groups corroborating the formation of the divalent species. In **Py4CPDTV** treatment with TFA of the radical cation generates a species with a strong absorption at 1504 nm which also correlates with the band at 1402 nm in the dication of the parent molecule without end-capping vinyl pyridine groups (the same spectra are obtained upon sequential oxidation with $FeCl_3$). In general, the optical gaps from the absorption spectra of the neutral, bisprotonated, radical cation and dications forms of the studied compounds show a continuous decrease of these values as the molecular size increases revealing the good conditions for π-electron and charge delocalization in the **Py*n*CPDTV** oligomers.

Oxidation of oligothiophenes[28] by TFA has been described to form radical cations by action of photo-activated oxygen mediated by the formation of singlet oxygen which produces the oxidation of the oligothiophene generating anionic oxygen. The role of the strong acid is to protonate the oxygen anion thus displacing the reaction towards the quantitative generation of the oxidized oligothiophenes. Alternatively, it has been reported the oxidation of ferrocene[29] by strong acid such as TFA which can directly proceed by reduction of the acid to its corresponding aldehyde. Both of these mechanisms can be acting in the oxidation of our compounds. However, in our case, the process of oxidation with TFA starts by rapid bisprotonation of the pyridines, which is the reactant that upon TFA excess

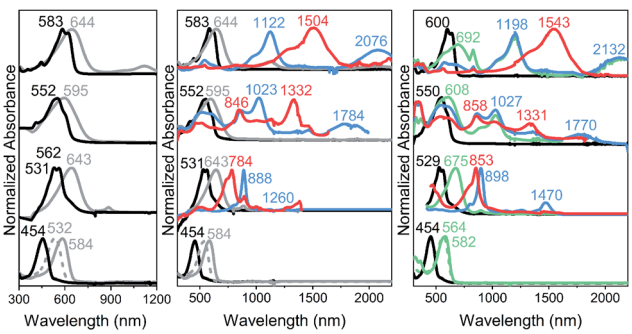

Fig. 2 From bottom to top: Py1CPDTV, Py2CPDTV, Py3CPDTV and Py4CPDTV. Left: electronic absorption spectra of neutral and bisprotonated compounds; middle: electronic absorption spectra upon excess treatment with TFA; and right: upon chemical oxidation with $FeCl_3$. The color codes are: black lines, neutrals; grey lines, bisprotonated; green lines, Fe(III)-bicoordinated; light blue lines, radical cations; and red lines, dications.

converts to cations and dications. This is summarized in Scheme 3 for the case of oxidation with TFA through the aldehyde mechanism.

Optical properties in thin films: vapochromism. Fig. 3 and S40–S42† display the absorption spectra of the studied compounds in spin-coated thin films as formed, and after treatment with TFA vapors from a concentrated TFA solution in water.

The corresponding absorption spectra of the as formed thin films are fully consistent with the neutral spectra in solution showing additional broadening due to the solid-state interactions. Upon exposition to TFA vapors, a very fast change (within seconds) of the colors of all samples was observed. Trying to analyze the reversibility, the vapor-treated thin films were exposed to NH_3 vapors and the spectra of the pristine materials were almost fully recovered. For instance, in **Py3CPDTV** the recovery is complete, whereas for **Py4CPDTV** the final spectrum still differs from the initial. In this regard, the Raman spectra taken before and after TFA/NH_3 treatments of **Py3CPDTV** are essentially identical reveling that apart from the different kinetics of the protonation/deprotonation processes, no structural damage has occurred.

Electrical properties: organic field-effect transistors. The inclusion of pyridines to the **CPDTV** cores enables to protonation and oxidation both being carried out by TFA, or dual dopant action, either protonic or electronic that is now studied in electrical devices (*i.e.*, in field-effect transistors). Table 2 summarizes the electrical data for **Py3CPDTV** and **Py4CPDTV** semiconductors.

Modest on-currents of the pristine samples (5.03×10^{-9} A and 1.88×10^{-8} A) are obtained, which can be justified by the low crystallinity of the samples.[26] Field effect mobilities were calculated using the equation describing the *I–V* characteristics of a field-effect transistor in saturation regime, registering hole transport for both compounds with mobilities values of 3.2×10^{-6} cm^2 V^{-1} s^{-1} and 2.6×10^{-4} cm^2 V^{-1} s^{-1}, for **Py3CPDTV** and **Py4CPDTV**, respectively. Threshold voltages are found to be positive due to unintentional doping by oxygen/water, implying that the films are somewhat conductive even when no gate voltage is applied.[27,28] Nonetheless, films deposited for OFET purposes were exposed to TFA vapors for 5–10 seconds and 1 hour, and the devices characteristics were measured (Fig. 4 and S43†). Even after very low exposition times, the on-currents remarkably increase up to 2 orders of magnitude (Table 2 and Fig. 4) disclosing off-currents with high values, indicating that the films are also likely electronically-doped quickly upon exposition to TFA vapor, in line with a fast chemical doping.[28]

The recorded output plots (Fig. S43†) present a linear shape, showing some modulation of the current with gate voltage; however, saturation regime is not reached even at high source-drain voltages. These linear output plots have been previously recorded in doped organic semiconductors[29] and preclude any measurement of accurate device characteristics at saturation conditions. Interestingly, these TFA doped films are also responsive to the inversion of the bias voltage and the same substrate of TFA doped **Py4CPDTV** also shows remarkable currents of $\sim 2 \times 10^{-6}$ A at positive gate voltages, indicating electron transport at very short exposition times of ~10 s to TFA (Fig. S44†). Comparing current intensities at both bias in TFA doped **Py4CPDTV**, we can assure that both are rather well balanced ($\sim 2 \times 10^{-6}$ A). This ambipolar charge transport in doped **Py4CPDTV** is in accord with the enhanced electron acceptor character of the bis-protonated compounds and with the simultaneously generation of radical cations by TFA acid.

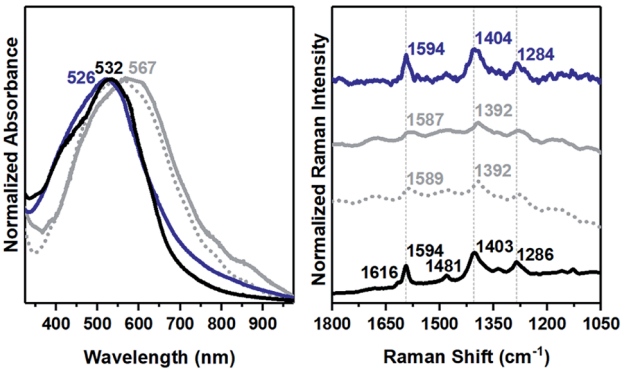

Fig. 3 (Left) Electronic absorption spectra of spin-coated thin films of Py3CPDTV (black line), upon treatment with TFA acid (dashed and solid grey lines at different exposition times) and the recovered spectrum upon treatment with NH_3 vapor (dark blue line). (Right) The corresponding 1064 nm FT-Raman spectra.

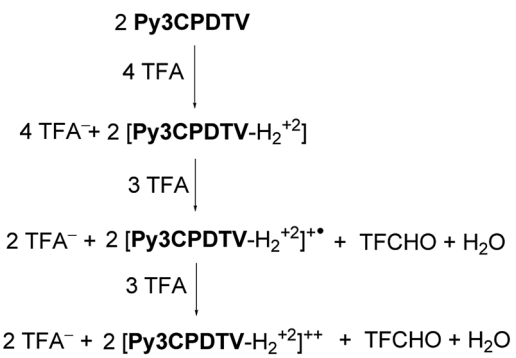

Scheme 3 Oxidation reaction of Py3CPDTV with TFA forming the corresponding trifluoroacetaldehyde (TFCHO) and water.

Table 2 OFET absolute on-current data at negative bias and transistor parameters (when possible, in pristine films) for OTS solution-processed films of the indicated semiconductors annealed at 80 °C and measured in air

	t_{exp} [a]	I_{max} (A)	μ_h (cm^2 V^{-1} s^{-1})	V_T (V)
Py3CPDTV[b]	Pristine	5.03×10^{-9}	3.20×10^{-6}	29
	5–10 s	1.10×10^{-7}		
	1 h	2.60×10^{-7}		
Py4CPDTV[c]	Pristine	1.88×10^{-8}	2.60×10^{-4}	13
	5–10 s	3.87×10^{-6}		
	1 h	2.77×10^{-6}		

[a] Exposition time to TFA. [b] Spin-coated films. [c] Drop-coated films.

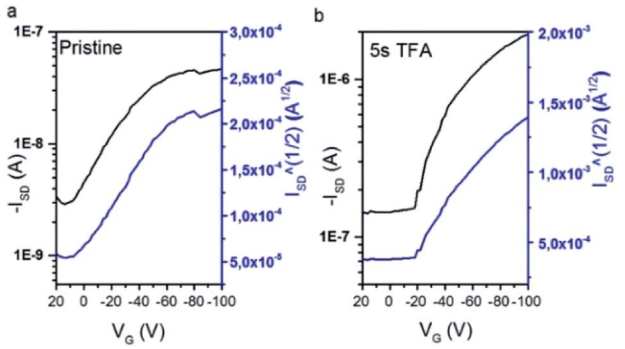

Fig. 4 I_{SD}–V_G plot data for **Py4CPDTV**-based devices at negative bias. (a) Pristine film and (b) after exposition to TFA for 5–10 s.

Single-molecule conductance

The inclusion of pyridines to the **CPDTV** cores affords the ability to coordinate to Fe(III) and other metals such as gold. Conveniently, this allows one to form metal-molecule junctions in which single-molecule conductance measurements can be carried out. Owing to their good π-electron delocalization, the **Py*n*CPDTV** series may serve as effective molecular wires. Using the STM-BJ technique, we found that the **Py*n*CPDTV** series are highly conductive, considering the length of the oligomers.

Empirically, conductance tends to decay exponentially with molecule length. This trend arises from a simple tunneling model wherein the molecule represents a potential barrier that the electrons must tunnel. The tunneling probability for electrons to cross the barrier decreases exponentially with barrier length. Due to this exponential decay, long, oligomeric compounds typically serve as poor single-molecule conductors. However, if the molecule contains energy levels that are close to the Fermi energy of the electrodes, electrons may resonantly tunnel through these orbitals with a much higher probability. Accordingly, a higher conductance will be measured and the exponential decay model will no longer hold.

We measured the single-molecule conductance of the **Py*n*CPDTV** series at high bias (750 mV, Fig. 5). High conductance values are observed for **Py2CPDTV** ($10^{-2.4}$ G_0), **Py3CPDTV** ($10^{-2.6}$ G_0), and **Py4CPDTV** ($10^{-3.2}$ G_0). These conductance values are extracted from the peak positions in the 1D histograms (Fig. 5, inset). In the 2D histograms (Fig. 5), we see that the average plateau length of the conductance traces increases with molecule length. Understandably, a longer molecule can bridge a longer electrode gap. Therefore, the plateau length is expected to correlate with molecule length. However, the plateau length will always be an underestimate of the true molecule length due the elastic relaxation of the electrodes upon rupture of the gold–gold point contact.[30] With this in mind, the observed plateau lengths are consistent with the length of the molecules, which indicates that the molecules are bound to the electrodes through the end-capped pyridine groups. Impressively, **Py4CPDTV** mediates electron transport at a conductance of ~10^{-3} G_0 over a length of ~5 nm (nitrogen–nitrogen length obtained from DFT calculations). These high conductance values are consistent with resonant transport, whereby the HOMO or LUMO level lies within the bias window and the associated molecular orbital is highly delocalized.

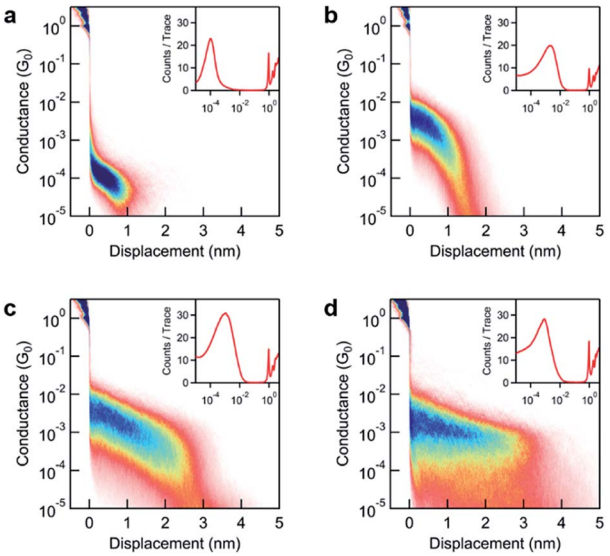

Fig. 5 2D histograms compiled from 5000 traces, measured at a bias of 750 mV for (a) **Py1CPDTV** (b) **Py2CPDTV** (c) **Py3CPDTV** and (d) **Py4CPDTV**. The reported conductance values are calculated from the peak positions in the 1D histograms (inset).

The conductance of **Py1CPDTV** is considerably lower ($10^{-4.0}$ G_0, Fig. 6a). We ascribe the lower conductance to the larger HOMO–LUMO gap, which makes the HOMO and LUMO levels (Table 1) inaccessible within the bias window at both low and high bias. Conductance is therefore through a non-resonant process for this molecule. This is consistent with the fact that the peak conductance of **Py1CPDTV** does not change with bias. Since HOMO–LUMO gap decreases with oligomer length,[31] the HOMO and LUMO levels should become increasingly accessible for the longer oligomers. Indeed, for **Py2CPDTV**, a dramatic increase in conductance is observed with increasing bias as one of these levels enters into the bias window and resonant transport is achieved (Fig. 6b). Owing to resonant transport, we can drive higher currents through the longer oligomers in the **Py*n*CPDTV** series than can be achieved for traditional conjugated oligomers of similar length.

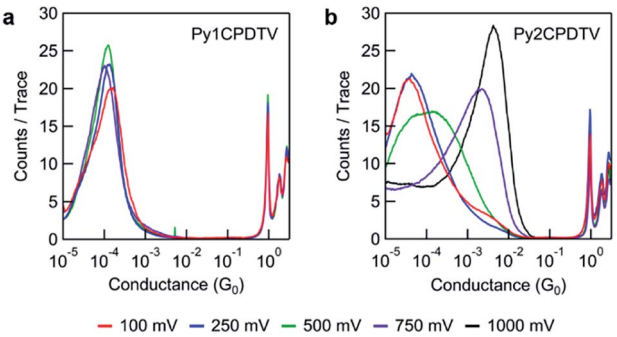

Fig. 6 1D Histograms compiled from 5000 traces for (a) **Py1CPDTV** and (b) **Py2CPDTV** at different biases. The conductance of **Py1CPDTV** remains fixed with bias, whereas a large increase in conductance with bias is observed for **Py2CPDTV**.

Conclusions

A new series of four oligomers of cyclopentadithiophene-vinylenes end capped with vinyl-pyridine groups was synthesized and their optical and electronic properties were studied by spectroscopic techniques and electrochemistry. We found that the neutral molecules can be easily protonated by TFA. The mechanism and consequences on the electronic properties of the molecules have been also addressed. The action of TFA not only consists of the acid–base reaction with the nitrogens, but we also detected and explored that further excess treatment with TFA provokes the oxidation of the conjugated core generating radical cations and dications. The same analysis was studied and confirmed to occur in the solid state, which gives way to test these substrates in electrical devices such as OFETs. The semiconducting properties of these molecules either as neutral and as upon treatment with TFA have been reported in which we found that the electrical response is sensitive to the treatment with TFA. In addition, since TFA produces species of these oligomers able to stabilize electrons, and hole is reported for the same substrate. Finally, the characterization is completed with the study of single molecule conductance in break junction devices. We found outstanding behavior of the molecules as molecular wires due to the control of the transport by resonance with the molecular orbitals which mediate very efficient and large transport to distances as large as 5 nm. This study reveals the interesting modulation of properties of π-conjugated molecules by the appropriate selection of end-capping groups and how this can open new perspectives coming from already existing and well known molecules.

Conflicts of interest

There are no conflicts to declare.

Acknowledgements

We thank MINECO/FEDER of the Spanish Government (CTQ2015-69391-P and PGC2018-098533-B-I00), the Research Central Services (SCAI) of the University of Málaga for the access to the facilities. SMR acknowledges MINECO for a FPI predoctoral grant.

Notes and references

1 P. Mayorga-Burrezo, R. Domínguez, J. L. Zafra, T. M. Pappenfus, P. de la Cruz, L. Welte, D. E. Janzen, J. T. López-Navarrete, F. Langa and J. Casado, *Chem. Sci.*, 2017, **8**, 8106.

2 J. Roncali, *Acc. Chem. Res.*, 2000, **33**, 147; I. Jestin, I. P. Frère, P. Blanchard and J. Roncali, *Angew. Chem., Int. Ed.*, 1998, **37**, 942.

3 I. F. Perepichka and D. F. Perepichka, *Handbook of Thiophene-Based Materials: Applications in Organic Electronics and Photonics*, Wiley, Chichester, U.K., 2009; L. Zhang, N. S. Colella, B. P. Cherniawski, S. C. B. Mannsfeld and A.-L. Briseno, *ACS Appl. Mater. Interfaces*, 2014, **6**, 5327.

4 H. N. Tsao, D. M. Cho, I. Park, M. R. Hansen, A. Mavrinskiy, D. Y. Yoon, R. Graf, W. Pisula, H. W. Spiess and K. Müllen, *J. Am. Chem. Soc.*, 2011, **133**, 2605; M. Zhang, M. H. N. Tsao, W. Pisula, C. Yang, A. K. Mishra and K. Müllen, *J. Am. Chem. Soc.*, 2007, **129**, 3472.

5 H.-R. Tseng, H. Phan, C. Luo, M. Wang, L. A. Perez, S. N. Patel, L. Ying, E. J. Kramer, T.-Q. Nguyen, G. C. Bazan and A. J. Heeger, *Adv. Mater.*, 2014, **26**, 2993.

6 M. Khatib, T.-P. Huynh, J. J. Sun, T. T. Do, P. Sonar, F. Hinkel, K. Müllen and H. Haick, *Adv. Funct. Mater.*, 2019, **29**, 1808188.

7 J. Lee, S.-H. Kang, S. M. Lee, K. C. Lee, H. Yang, Y. Cho, D. Han, Y. Li, B. H. Lee and C. Yang, *Angew. Chem., Int. Ed.*, 2018, **57**, 13629.

8 Y.-Q. Yi, H. Feng, N. Zheng, X. Ke, B. Kan, M. Chang, Z. Xie, X. Wan, C. Li and Y. Chen, *Chem. Mater.*, 2019, **31**, 904.

9 S. Aghazada, P. Gao, A. Yella, G. Marotta, T. Moehl, J. Teuscher, J.-E. Moser, F. Angelis, M. Gratzel and M. K. Nazeeruddin, *Inorg. Chem.*, 2016, **55**, 6653.

10 D.-Y. Chen, Y.-Y. Hsu, H.-C. Hsu, B.-S. Chen, Y.-T. Lee, H. Fu, M.-W. Chung, S.-H. Liu, H.-C. Chen, Y. Chi and P.-T. Chou, *Chem. Commun.*, 2010, **46**, 5256.

11 Y. Bai, J. Zhang, D. Zhou, Y. Wang, M. Zhang and P. Wang, *J. Am. Chem. Soc.*, 2011, **133**, 11442.

12 S.-W. Chang and M. Horie, *Chem. Commun.*, 2015, **51**, 9113.

13 S.-T. Chiu, H.-Y. Chiang, Y.-Y. Lu, H. Tanaka, T. Hosokai and M. Horie, *Chem. Commun.*, 2018, **54**, 5546.

14 J. M. Beebe, V. B. Engelkes, L. L. Miller and C. D. Frisbie, *J. Am. Chem. Soc.*, 2002, **124**, 11268; C. Zhou, M. R. Deshpande, M. A. Reed, L. Jones and J. M. Tour, *Appl. Phys. Lett.*, 1997, **71**, 611.

15 S. T. Purcell, N. Garcia, V. T. Binh, L. J. II and J. M. Tour, *J. Am. Chem. Soc.*, 1994, **116**, 11985; J. M. Tour, L. Jones, D. L. Pearson, J. J. S. Lamba, T. P. Burgin, G. M. Whitesides, D. L. Allara, A. N. Parikh and S. V. Atre, *J. Am. Chem. Soc.*, 1995, **117**, 9529.

16 H. E. Katz, A. Dodabalapur and Z. Bao, *Oligo- and Polythiophene Field Effect Transistors*, ed. D. Fichou, Wiley, Weinheim, 1999.

17 I. F. Perepichka, D. F. Perepichka, H. Meng and F. Wudl, *Adv. Mater.*, 2005, **17**, 2281.

18 S. C. Rasmussen, S. J. Evenson and C. B. McCausland, *Chem. Commun.*, 2015, **51**, 4528.

19 A. Mishra, C.-Q. Ma and P. Baeuerle, *Chem. Rev.*, 2009, **109**, 1141.

20 J. H. Schön, H. Meng and Z. Bao, *Nature*, 2001, **413**, 713.

21 B. R. Baker and M. H. Doll, *J. Med. Chem.*, 1971, **14**, 793.

22 M. J. Frisch, G. W. Trucks, H. B. Schlegel, G. E. Scuseria, M. A. Robb, J. R. Cheeseman, G. Scalmani, V. Barone, G. A. Petersson, H. Nakatsuji, X. Li, M. Caricato, A. V. Marenich, J. Bloino, B. G. Janesko, R. Gomperts, B. Mennucci, H. P. Hratchian, J. V. Ortiz, A. F. Izmaylov, J. L. Sonnenberg, D. Williams-Young, F. Ding, F. Lipparini, F. Egidi, J. Goings, B. Peng, A. Petrone, T. Henderson, D. Ranasinghe, V. G. Zakrzewski, J. Gao, N. Rega,

G. Zheng, W. Liang, M. Hada, M. Ehara, K. Toyota, R. Fukuda, J. Hasegawa, M. Ishida, T. Nakajima, Y. Honda, O. Kitao, H. Nakai, T. Vreven, K. Throssell, J. A. Montgomery Jr, J. E. Peralta, F. Ogliaro, M. J. Bearpark, J. J. Heyd, E. N. Brothers, K. N. Kudin, V. N. Staroverov, T. A. Keith, R. Kobayashi, J. Normand, K. Raghavachari, A. P. Rendell, J. C. Burants. S. Iyengar, J. Tomasi, M. Cossi, J. M. Millam, M. Klene, C. Adamo, R. Cammi, J. W. Ochterski, R. L. Martin, K. Morokuma, O. Farkas, J. B. Foresman and D. J. Fox, *Gaussian 16, Revision B.01*, Gaussian, Inc., Wallingford CT, 2016.

23 A. D. Becke, *J. Chem. Phys.*, 1993, **98**, 1372.

24 M. M. Francl, W. J. Pietro, W. J. Hehre, J. S. Binkley, M. S. Gordon, D. J. Defrees and J. A. Pople, *J. Chem. Phys.*, 1982, **77**, 3654.

25 S. R. Walter, J. Youn, J. D. Emery, S. Kewalramani, J. W. Hennek, M. J. Bedzyk, A. Facchetti, T. J. Marks and F. M. Geiger, *J. Am. Chem. Soc.*, 2012, **134**, 11726.

26 B. Q. Xu and N. J. J. Tao, *Science*, 2003, **301**, 1221.

27 L. Venkataraman, J. E. Klare, C. Nuckolls, M. S. Hybertsen and M. L. Steigerwald, *Nature*, 2006, **442**, 904.

28 Y. Yu, E. Gunic and L. L. Miller, *Chem. Mater.*, 1995, **7**, 255.

29 T. E. Bitterwolf and A. C. Ling, *J. Organomet. Chem.*, 1972, **40**, C29.

30 H. N. Tsao, D. M. Cho, I. Park, M. R. Hansen, A. Mavrinskiy, D. Y. Yoon, R. Graf, W. Pisula, H. W. Spiess and K. Müllen, *J. Am. Chem. Soc.*, 2011, **133**, 2605.

31 Y. Zang, S. Ray, E. Fung, A. Borges, M. H. Garner, M. L. Steigerwald, G. C. Solomon, S. Patil and L. Venkataraman, *J. Am. Chem. Soc.*, 2018, **140**, 13167.